Hierarchical Porous Carbon Materials Derived from Microwave-assisted Heating of Zeolitic Imidazolate Frameworks for Use as Supercapacitor Electrodes

J Z Zou[1,2], S Y Liu[1], H L Wu[1,*], Q Luo[1], L Huang[1,3], X R Zeng[1,2], J Ma[1], Y C Yao[1], Q Zhang[4] and B L Peng[1]

[1] Shenzhen Key Laboratory of Special Functional Materials & Shenzhen Engineering Laboratory for Advance Technology of ceramics, College of Materials Science and Engineering, Shenzhen University, Shenzhen, 518060. P.R. China

[2] Guangdong JANUS Intelligent Group Corporation Limited, Dongguan, 441900, P.R. China

[3] Key Laboratory of Optoelectronic Devices and Systems of Ministry of Education and Guangdong Province, College of Optoelectronic Engineering, Shenzhen University, Shenzhen 518060, P.R. China

[4] School of Aerospace, Transport and Manufacturing, Cranfield University, Cranfield, Bedfordshire, MK43 0AL, UK

Corresponding author and e-mail: H L Wu, whl@szu.edu.cn

Abstract. A series of hierarchically structured nanoporous carbons are prepared via the direct carbonization of zeolitic imidazolate frameworks (ZIF-8) using a microwave-assisted heating method for the first time. The results indicate that the microwave carbonization temperature has a remarkable influence on the surface area and pore structure of the obtained porous carbons. ZIF-8 provides the carbon and the microporous structure. Significant numbers of mesopores and macropores emerge in the samples carbonized at high temperatures, indicating a clear difference from carbons prepared using traditional heating methods. The resulting porous carbons possess surface areas ranging from 384.4 to 947.5 m^2 g^{-1} and pore volumes ranging from 0.17 to 0.49 cm^3 g^{-1}. For a carbonization temperature of 1000 °C, the porous carbon possesses the largest specific capacitance of 207.7 F g^{-1} at 0.1 A g^{-1} and the highest retention of 66.5% when the current density increases from 0.1 to 10 A g^{-1}, which should be attributed to the proper hierarchical pore structure and the relatively high graphitization degree.

1. Introduction

Due to the rapid consumption of fossil fuel resources and associated environmental problems, research into efficient energy storage systems has attracted considerable interest. Among the various energy storage devices, compared to traditional batteries, supercapacitors have attracted more and more attention due to their high power densities, fast charging and discharging characteristics, long cycle lives, less environmental pollution, etc. These devices have been widely used in digital devices, electric vehicles, communication technologies and other fields [1-3]. Research has been focused on

increasing the energy density of supercapacitors without weakening the high power density and stable cyclic life. Currently, nanoporous carbon (NPC) materials are identified as one of the most promising candidates for supercapacitor electrode materials due to their high thermal and chemical stabilities, large specific surface areas, controllable pore structures, high conductivities, easy manufacturing in large quantities with relatively low costs, etc [4-6]. In the electrochemical capative performance, the pore size distributions of the porous carbons play an important role, and a hierarchical pore structure with well-interlinked small and large pores is regarded to provide new accesses to improve both the specific capacitances and rate capabilities of porous carbons as supercapacitor electrodes [7-12]. As a result, many approaches have been studied to prepare highly porous carbons and adjust their pore structures, including laser ablation [13], chemical vapour decomposition (CVD) [14], arc discharging [15] and templating [16,17], as well as physical or chemical activation methods [18]. Among these methods, the template method has become one of the most studied approaches for the preparation of nanoporous carbons due to its regulated architecture, relatively narrow pore size distribution, and desirable physicochemical properties [19]. However, the templating process requires additional pore-forming templates and acid treatment steps to remove the templates, which result in enhancement of preparation cost and difficulty of utilization for large-scale production.

To solve these major problems, a class of novel porous materials, crystalline metal-organic frameworks (MOFs), have attracted an enormous amount amount of attention because they can act as excellent precursors or sacrificial templates for the preparation of nanoporous carbons (NPCs) due to their extremely high specific surface areas, favourable thermal stabilities, tailored pore structures and adjusted channels [20-23]. Importantly, MOFs can act as both the templates and the carbon sources, thus reducing the producing and purifying steps to obtain the resulting porous carbon.

Currently, it is widely used for the carbonization technique to prepare hierarchically nanoporous carbons by selecting appropriate carbon sources or precursors. However, this kind preparation method of nanoporous carbons is still unfavourable because there is always a very slow heating rate with the conventional heating techniques (tube furnace), which makes the carbonization expensive and difficult to scale up. Moreover, carbon materials prepared in this way can only generate similar pore structures to the MOFs precursors, lacking variety if there is no other treatment. Microwave-assisted heating, which arises from the direct interaction of matter with electromagnetic energy, has attracted an increasing attention due to its potential advantages over traditional heating techniques [24]. These advantages include a remarkable decrease in heat-up time, a smaller requirement of energy, fewer steps involved in the heating process, a more sensitive and efficient operating system, etc. The final samples obtained from the microwave-assisted heating method will most likely be more economically competitive than those obtained using conventional methods [25].

In this work, we choose ZIF-8 as a precursor for the preparation of nanoporous carbons using a microwave-assisted heating method. The approach presented here does not require any addition of carbon sources or pore-forming templates. Furthermore, the surface area and pore structure are easily regulated by controlling the microwave carbonization temperature. The resulting ZIF-derived nanoporous carbons are comprehensively characterized using a varieties of techniques. It is discussed in detail for the structural evolution of the nanoporous carbons with increasing temperature and their electrochemical behaviour as electrode materials for supercapacitors.

2. Experimental section

2.1. Preparation of ZIF-8

ZIF-8 powder was synthesized on the basis of the method reported in the literature [26]. All chemicals were purchased from Aladdin Chemical Co (Shanghai China). First, 2.62 g of zinc nitrate hexahydrate ($Zn (NO_3)_2 \cdot 6H_2O$) was dissolved in 100 mL of methanol to form solution A, and 5.79 g

of 2-methylimidazole (MmIm) was dissolved in 100 mL of methanol to generate solution B. Then, two solutions above were mixed up and stirred for 1 h at room temperature. After that, the resulting milky solution was centrifuged at 10000 rpm for 5 min, and the supernatant was removed. The precipitates was washed with methanol and centrifuged again. The whole process was repeated twice. The resulting powder was dried in an oven at 60 ℃ overnight.

2.2. Preparation of nanoporous carbon (NPC)

Five nanoporous carbons were prepared from direct carbonization of ZIF-8 using a microwave-assisted heating method as follows: First, a quartz tube with 0.8 g of dried ZIF-8 powder was inserted into an alumina crucible filled with SiC powder (a microwave absorber), which has a critical auxiliary heating effect. Then, the whole alumina crucible was wrapped with asbestos and placed in a microwave furnace. The furnace was heated up to the required carbonization temperature (600, 700, 800, 900 or 1000 °C) at a very high rate of heating (generally within 5 min) under a nitrogen atmosphere with a gas pressure of 20 kPa. Then the target temperature was maintained for 3 h, followed by cooling to room temperature in nitrogen. After treated with an aqueous solution of HCl (0.1 M) to remove Zn or ZnO residue from the decomposition of ZIF-8 template, the as-prepared nanoporous carbon materials were denoted as NPC-600, NPC-700, NPC-800, NPC-900, and NPC-1000 respectively. For comparison, another carbon sample was obtained by direct carbonization of ZIF-8 using a tube furnace. Firstly, the furnace was filled with nitrogen gas at room temperature. Then, the furnace was heated up to 1000 °C at a conventional rate of 5 °C/min and held at 1000 °C for 3 h. After the furnace was cooled to room temperature in nitrogen, the carbon sample was treated with 0.1 M HCl and labelled as NPC-T-1000.

2.3. Characterization

X-ray diffraction (XRD) patterns were obtained on a Bruker D8 advance powder X-ray diffractometer using Cu Kα radiation (20 kV, 200 mA, λ=1.54178 Å) with a step size of 0.02° and step time of 0.5 s. Scanning electron microscopy (SEM) images were examined using a Hitachi SU-70 scanning electron microscope at an acceleration voltage of 20 kV. Nitrogen adsorption-desorption curves were recorded using a micrometrics ASAP 2020 instrument at liquid nitrogen temperature (77 K). All samples were degassed at 523 K for 4 h before measurement. The Brunauer-Emmett-Teller (BET) surface areas were calculated from the nitrogen isotherm curves ranging from the relative pressure of 0 to 0.3. The total pore volumes were determined from the amount of nitrogen adsorbed at P/P_0 of ca. 0.99. The pore size distributions (PSDs) were determined using a density functional theory (DFT) method. The micro- and mesopore volumes were obtained using adsorption isotherms from a DFT method, and the macropore volumes were determined by subtracting the micro- and mesopore volumes from the total pore volume. Transmission electron microscope (TEM) images were obtained using a Joel JEM-2100 at an acceleration voltage of 100 kV. Laser Raman spectroscopy was performed on a Renishaw inVia Reflex.

2.4. Electrode preparation and electrochemical performance test

All electrochemical performances were examined on a standard three-electrode electrochemical station,
which was equipped with a counter electrode of Pt, a reference electrode of Hg/HgO, and a working electrode of ZIF-derived nanoporous carbon in 6 M KOH. The working electrode was prepared by mixing up ZIF-derived nanoporous carbon (85 wt%), acetylene black (10 wt%) and polytetrafluoroethylene (5 wt%) with moderate ethanol to form slurry and then coat onto a nickel foam with a coating area of 1 cm², The foam was dried at 110 °C in vacuum oven overnight, Then, in

order to completely adhere with the electrode material, the foam was pressed under a pressure of 10 MPa. The mass loading of active materials on the prepared working electrode is nearly 5 mg cm^{-2}.

All electrochemical experiments were performed at ambient temperature on a CHI660e electrochemical workstation (Shanghai Chenhua Instruments Co.). Before the measurements, the working electrodes were soaked in electrolyte for half an hour so that the active materials could be fully infiltrated by the electrolyte. The primary testing method was cyclic voltammetry (CV) at different scan rates ranging from 5 to 200 mV s^{-1}. Galvanostatic charge/discharge (GC) measurements were also performed at different current densities raging from 0.1 A g^{-1} to 10 A g^{-1} in the potential range of -1.0~0 V. Electrochemical impedance spectra (EIS) were measured over the frequency ranging from 100 kHz to 0.01 Hz with an alternate current perturbation of 5 mV at open circuit voltage. The EIS data were analysed using Nyquist plots with the real part (Z') and imaginary part (Z") of impedance marked as the X-axis and Y-axis, respectively.

For galvanostatic charge/discharge processes, the specific capacitances were calculated using the following equation[27]: $C_m = I\Delta t(m\Delta V)^{-1}$. In this equation, C_m (F g^{-1}) is the specific capacitance, I (A) represents the discharge current, Δt (s) represents the discharge time, m (g) refers to the mass of active material on the electrode, and ΔV (V) is the voltage change within the discharge time.

3. Results and discussion

3.1. Structure and texture characterization

Figure 1 shows the XRD and SEM images of as-synthesized ZIF-8. The XRD pattern of ZIF-8 powder is in great agreement with the simulation, suggesting that the ZIF-8 material has been synthesized successfully [28]. And the SEM image shows a typical rhombic dodecahedron morphology of ZIF-8 with a particle size of approximately 100 nm.
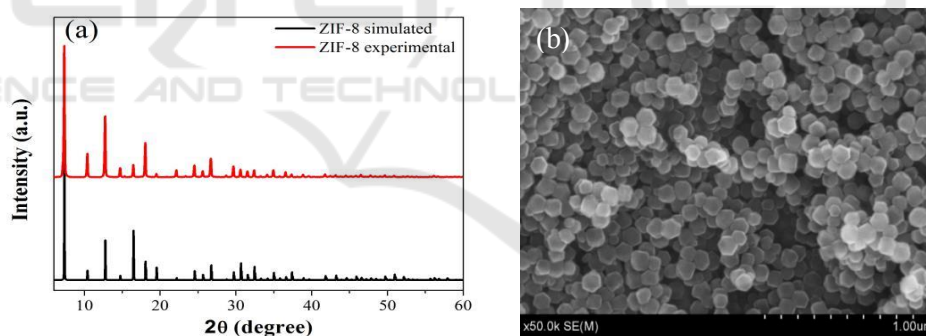

Figure 1. (a) XRD pattern and SEM image of ZIF-8.

XRD patterns of NPC-600, NPC-700, NPC-800, NPC-900, NPC-1000 and NPC-T-1000 are shown in Figure 2a. As we can see, after carbonization, all of the resulting porous carbon samples lose the characteristic XRD peaks of the parental ZIF-8, and display two broad peaks at 2θ = 23° and 44°, which are corresponding to the (002) and (101) planes of graphitic carbon. The (002) refers to a graphite-like peak, and (101) is related to the honeycomb lattice in single-layer graphene [29, 30]. Two broad diffraction peaks of NPC-1000 are the most noticeable among six ZIF-derived nanoporous carbon samples, indicating that NPC-1000 may hold better electrical conductivity and crystalline degree.
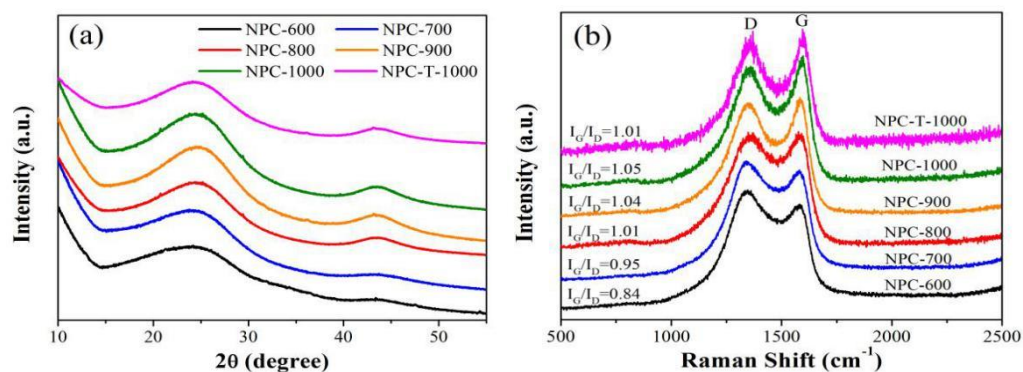
Figure 2. Powder XRD patterns and Raman spectra of six ZIF-derived nanoporous carbons.

To further study the graphitization degree of the six ZIF-derived nanoporous carbons, Raman spectra are given in Figure 2b. There are two featured broad peaks centered at approximately 1580 cm^{-1} and 1360 cm^{-1}, which are named the G band (graphite) and D band (disorder) respectively. The G band presents ideal graphitic sp^2 carbons, and the D band relates to disordered carbons [31, 32]. Generally, the graphitization degree of porous carbons can be estimated by comparing the relative intensity ratio of the G band to the D band (I_G/I_D) [33]. The ZIF-derived nanoporous carbon samples exhibited a gradual increase in I_G/I_D values from 0.84 to 1.05 as the microwave carbonization temperature increased from 600 to 1000 °C, indicating that these nanoporous carbons possess both graphitic and disordered structures [34] and a higher carbonization temperature contributes to the generation of graphitic sp^2 carbons. In addition, NPC-T-1000 achieves a lower I_G/I_D value than NPC-1000, which exhibits that microwaves are conducive to the formation of graphite carbon.
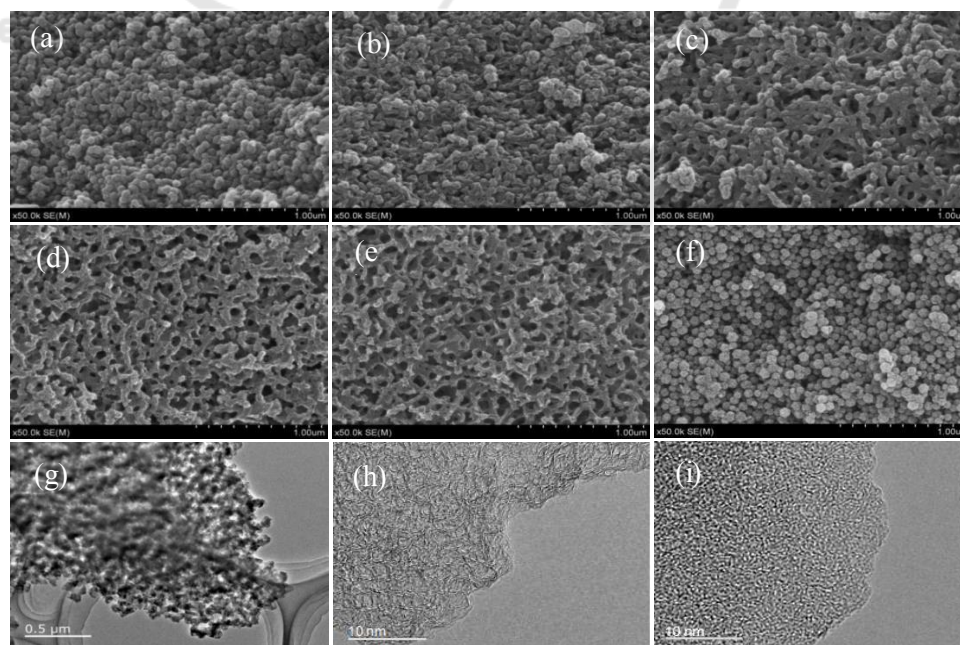
Figure 3. SEM images of six ZIF-derived nanoporous carbons: (a) NPC-600, (b) NPC-700, (c) NPC-800, (d) NPC-900, (e) NPC-1000, (f) NPC-T-1000 and representative TEM images of NPC-1000 (g, h) and NPC-T-1000 (i).

To explore the morphologies and structures of the six as-prepared ZIF-derived nanoporous carbon materials, both SEM and TEM analyses were performed. As shown in Figure 3, apparent morphological changes occur in the ZIF-derived nanoporous carbons. NPC-600 turns into spherical particles with a decreased particle size of approximately 75 nm, which is similar to NPC-T-1000. As the temperature increased to 800 °C, the sample cannot maintain the typical granular morphology well and undergoes particle bonding, forming interconnections between particles. In particular, for NPC-1000, instead of a typical granular morphology, a three-dimensional network morphology derived from interconnected particles has been adopted, generating obvious mesopores in the range of 30-40 nm and macropores in the range of 60-100 nm. Obviously, the morphologie and structure of NPC-1000 is quite distinct from the carbon material prepared by direct carbonization of ZIF-8 using a tube furnace [34, 35]. This indicates that the heating mode have important influence on the pore structure of carbon materials and the microwave-assisted heating process can be explained as follows: it generates a large amount of thermal energy when using microwave-assisted heating method to carbonize ZIF-8 at a very fast heating rate. Thus, the organic species of ZIF-8 are quickly decomposed, but the evacuating speed is far slower than the decomposing speed, so some of the released linkers or atoms return to form bonds with each other, which appear as macroscopic particle interconnections. As the temperature increased higher, large numbers of meso- and macropores appear due to the large improvement in the evacuating and decomposing efficiency of ZIF-8. Representative TEM images for NPC-1000 and NPC-T-1000 are presented in Figure 3 (g, h). Mesopores and macropores are clearly visible in NPC-1000, and the high-resolution TEM reveals that the sample possesses many micropores over the entire sample surface with a well-developed graphitic structure while NPC-T-1000 is nearly amorphous. The relatively high graphitization degree of NPC-1000 makes it a better electrical conductivity, which play an important role in electrochemical performance.

The nitrogen adsorption-desorption isotherms at 77 K (Figure 4a) were used to measure the specific surface areas and nanopores of the obtained porous carbons. At low relative pressure (P/P_0<0.1), all six porous carbons display significant nitrogen adsorption, which is in agreement with type I adsorption-desorption isotherm, indicating the development of microporosity. The isotherms for all the porous carbons are extremely similar, and the adsorption-desorption isotherm branches are almost reversible, indicating that all the carbons are predominantly microporous, which is corresponding to micropore structures presented in the parental ZIF-8 that acts as both the template and the carbon precursor [35]. In particular, for NPC-900 and NPC-1000, there appear hysteresis loops at high relative pressure (P/P_0>0.8), indicating the existence of partial mesopores or macropores in the carbons, which is in great agreement with the SEM and TEM results. It should be noted that NPC-T-1000 give the isotherm with a larger hysteresis loop than that of NPC-1000 over the relative pressure from 0.8 to 1.0. This is come from the interparticle space among the assembled small-sized particles rather than porosity in the material itself, which is invalid in electrochemical behaviour. The textural properties of the carbons are listed in Table 1. The BET surface areas and total pore volumes of six carbon samples are in the ranges of 384.4-1281.4 m^2 g^{-1} and 0.17-0.87 cm^3 g^{-1}. Among them, NPC-T-1000 shows the highest surface area of 1281.4 m^2 g^{-1}, and the largest total pore volume of 0.87 cm^3 g^{-1} due to the rich intergranular space. In comparison, NPC-1000 possesses lower values of 852 m^2 g^{-1} and 0.49 cm^3 g^{-1} respectively. The proportion of micropore surface area for the carbon materials using micro-assisted heating method is approximately 95%, and the proportion of mesopore and macropore volume varies from 35% to 41%. The relatively low micropore contributions for NPC-900 and NPC-1000 can be attributed to the complete decomposition of ZIF-8 and the formation of particle interconnections at high microwave carbonization temperature, leading to the formation of mesopores and macropores. NPC-1000 has the largest proportion of mesopore and macropore volume of 41%, which may make the sample a faster electron transfer.
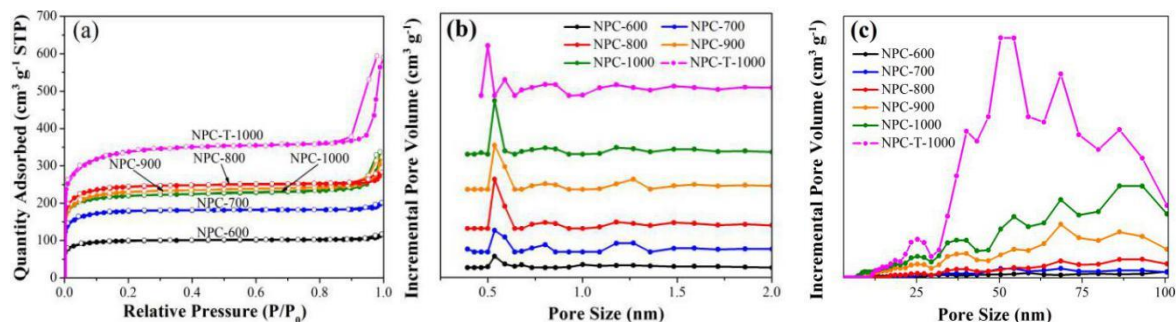
Figure 4. N_2 adsorption-desorption isotherms (a) and the corresponding pore size distributions of the ZIF-derived nanoporous carbons at different temperature, (b) micropore size distribution, (c) meso- and macropore size distribution.

To obtain more detailed information about the nanoporous structures, the pore size distributions (PSDs) (Figure 4b, c) were calculated using density functional theory based on the N_2 adsorption data. Five ZIF-derived nanoporous carbons using microwave-assisted heating exhibit narrow and sharp micropore size distribution centred at approximately 0.6 nm, while NPC-T-1000 suffers a smaller micropore size less than 0.5 nm. Small micropores may lead to low efficiency in capacitive performance, NPC-900 and NPC-1000 also possess macropores larger than 50 nm and mesopores of 20-50 nm. There are some other differences among the materials carbonized at different microwave carbonization temperatures. The PSD peaks of the samples carbonized at high temperature are higher than those of the low-temperature carbonized samples, and the micropore size of the carbons is slightly increased with increasing microwave carbonization temperature, indicating that the microwave holding temperature has a significant effect not only on the surface area and pore volume but also on the pore diameter and amount.

Table 1. Surface area, pore volume and capacitance of ZIF-derived nanoporous carbons.

Samples	surface area ($m^2\ g^{-1}$)		Pore volume ($cm^3\ g^{-1}$)			$C_m^{\ f}$ ($F\ g^{-1}$)
	$S_{BET}^{\ a}$	$S_{micro}^{\ b}$	$V_t^{\ c}$	$V_{micro}^{\ d}$	$V_{meso/macro}^{\ e}$	
NPC-600	384.4	367	0.17	0.11	0.06	109.6
NPC-700	693.1	669.4	0.30	0.23	0.07	149.9
NPC-800	947.5	906	0.42	0.32	0.1	194.3
NPC-900	886.9	832.2	0.47	0.29	0.18	201.1
NPC-1000	852	799.1	0.49	0.29	0.2	207.7
NPC-T-1000	1281.4	1161.9	0.87	0.41	0.46	181.5

[a] Brunauer-Emmett-Teller (BET) surface area.
[b] Microporous surface area.
[c] Total pore volume at $P/P_0=0.99$.
[d] Micropore volume.
[e] Mesopore and macropore volume.
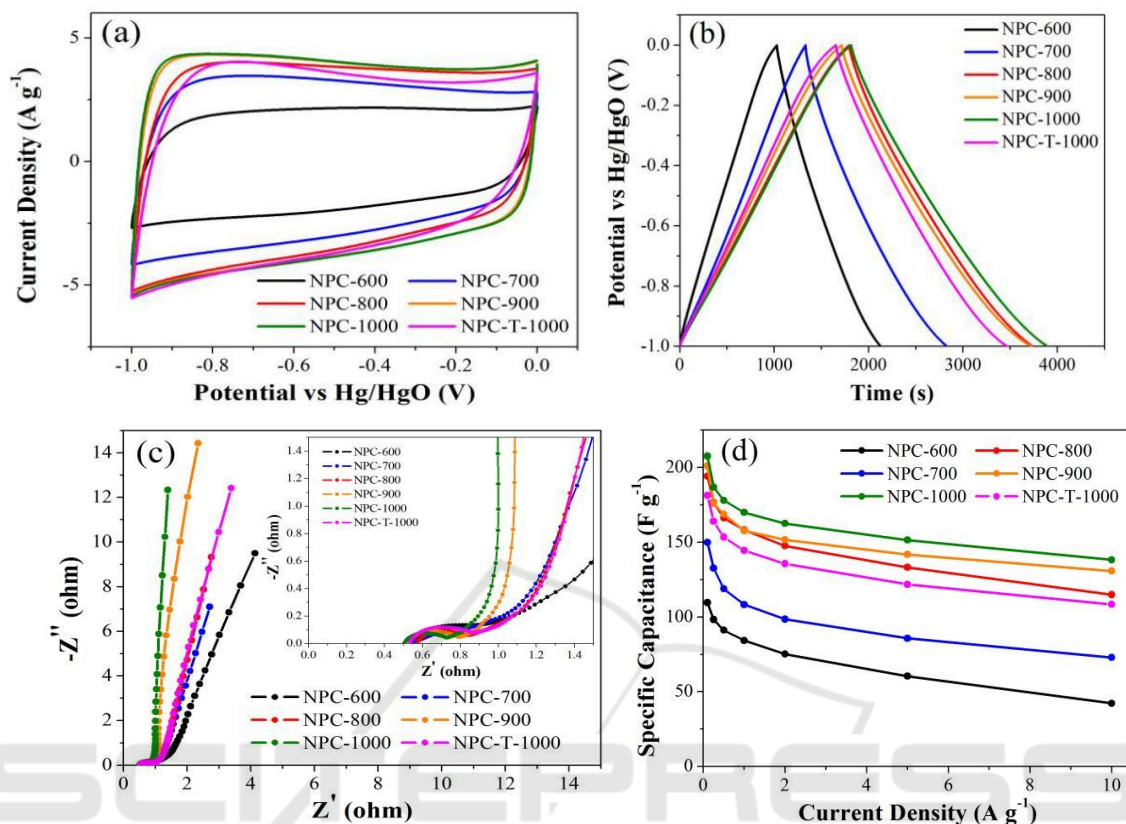[f] Specific capacitance at a current density of 0.1 A g^{-1}.

3.2. Electrochemical analysis

To investigate the capacitive performance of the six ZIF-derived nanoporous carbons, the CV, GC, and EIS were measured. The CV curves of the ZIF-derived nanoporous carbons at a scan rate of 25 mV s^{-1} are illustrated in Figure 5a, the cyclic voltammetry curves for all ZIF-derived nanoporous

carbons exhibit a nearly rectangular shape, which is typical behaviour for supercapacitors [36,37]. Compared to all other carbon samples, NPC-1000 shows the largest CV area and a more rectangular shape. The GC curves (Figrue 5b) at a current density of 0.1 A g^{-1} are symmetric, and NPC-1000 possesses the longest discharge time. The specific capacitances of the six nanoporous carbons are listed in Table 1, these values were calculated according to the discharge process. Obviously, NPC-1000 presents the largest capacitance value of 207.7 F g^{-1} compared to other porous carbons. This result presumably arises from both the higher percentage of graphitic carbons and the suitable hierarchical micro/meso/macropores structure of NPC-1000, which are advantageous for electrical conductivity and quick diffusion of electrolyte to the electrode [38-40]. It must be noted that although NPC-T-1000 possesses the largest value of surface area, its capacitance is only 181.5 F g^{-1}, which is even lower than the values of NPC-800 and NPC-900. The phenomenon reveals that capacitance is not in direct proportion to the specific surface area, there is only part of micropores are in effective use when the charge is transfered.

Figure 5c shows the electrochemical impedance spectroscopy, providing available details about the frequency responses of six ZIF-derived nanoporous carbons as supercapacitor electrode materials. In the high frequency region, the Nyquist plots exhibit depressed semicircles for the carbons (see the inset of Figrue 5c), which is related to the charge transport resistance between the electrode and electrolyte [41]. NPC-1000 shows a smallest crossing value of the Z' axis, which indicates that NPC-1000 has lower interfacial contact resistance, because NPC-1000 possesses a hierarchical pore structure, which is favourable for electrolyte ion migration. In the low frequency region, the larger the curve slope, the better the capacitive behaviour. A vertical curve indicates ideal capacitive behaviour and a fast transportation of the electrolyte ions in the nanopores of the carbon materials [42]. A shift of the vertical curve could result from the Warburg resistance for the electrolyte ions. Obviously, the EIS curve for NPC-1000 shows the largest value of curve slope, i.e., the lowest Warburg resistance, which demonstrates that NPC-1000 possesses the best electrical properties among the nanoporous carbons to act as an electrode material. The specific capacitances of six ZIF-derived nanoporous carbons at different current densities are presented in Figure 5d. Obviously, NPC-1000 shows the best capacitive performance. Detailedly, NPC-1000 shows the highest capacitance of 207.7 F g^{-1} at 0.1 A g^{-1}. Moreover, the capacitance of NPC-1000 still keep 66.5% when increasing the current density from 0.1 to 10A g^{-1}. In comparison, NPC-T-1000 achieves lower values of 181.5 F g^{-1} and 60.1% under the same test conditions. Obviously, NPC-1000 achieves the largest retention among the six nanoporous carbon samples.

To further study the electrochemical performance of NPC-1000, we performed a series of capacitive measurements at different current densities and different scan rates (Figure 6). Figure 6a exhibits the CV curves of NPC-1000 at different scan rates of 5, 10, 25, 50, 100 and 200 mV s^{-1}, all of them are in typical rectangular shape. At 200 mV s^{-1}, the CV curve suffers from some slight distortion, which may result from the limited mass transfer or ion transport [43]. As shown in Figure 6b, the triangle charge/discharge curves of NPC-1000 exhibit almost linear and symmetrical shapes at different current densities ranging from 0.1 to 10 A g^{-1}, indicating that the NPC-1000 electrode possesses good electrochemical reversibility [44]. The capacitance of NPC-1000 reaches 207.7 F g^{-1} at 0.1 A g^{-1}. It must be noted that this value is much larger than the ones of ZIF-8-derived nanoporous carbons using traditional carbonization method, like Z-800 derived from direct carbonization of ZIF-8 carbonized at 800 °C (130F g^{-1} at a scan rate of 50 mV s^{-1}) and Z-1000 at 1000 °C (112F g^{-1} at a scan rate of 50 mV s^{-1}) [31]. In addition, it was investigated and shown in Figure 6c for long-term cycle stability of NPC-1000 at a current density of 5 A g^{-1}. The capacitance of NPC-1000 keeps almost unchanged and only 4.7% of capacitance is lost after 1000 cycles, indicating that the material structures of NPC-1000 are very stable in the charge and discharge process.

Figure 5. Electrochemical properties of ZIF-derived nanoporous carbons. (a) Cyclic voltammetry curves at 25 mV s^{-1}, (b) galvanostatic charge and discharge curves at 0.1 A g^{-1}, (c) impedance spectroscopy, and (d) specific capacitance at different current densities.
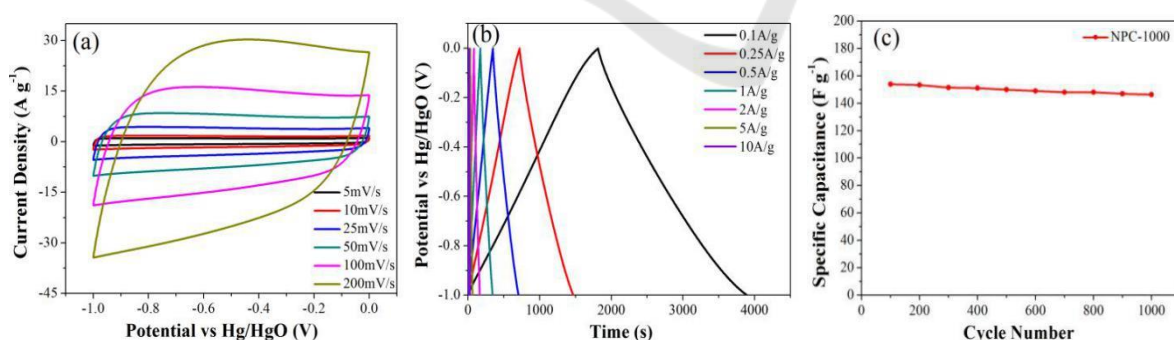
Figure 6. Capacitive performance of NPC-1000. (a) Cyclic voltammetry curves at different scan rates, (b) galvanostatic charge and discharge curves at different current densities, and (c) cycling stability at 5A g^{-1}.

Table 2. MOFs derived nanoporous carbons for supercapacitor.

Samples	BET (m^2 g^{-1})	Electrolyte	Scan rate (mV s^{-1})	Current density (A g^{-1})	Capacitance (F g^{-1})	Ref.
NPC-1000	838	6 M KOH		0.1	207.7	**this work**
Z-700	520	0.5M H_2SO_4	50	—	23	31
Z-800	720	0.5M H_2SO_4	50	—	130	31
Z-900	1075	0.5M H_2SO_4	50	—	128	31
Z-1000	1110	0.5M H_2SO_4	50	—	112	31
MC	1812	6M KOH/1.5M, NEt_4BF_4 acetonitrile	—	0.25	149/113	44
C800	2169	1 M H_2SO_4	5	—	188	45
C1000	3405	1 M H_2SO_4	5	—	161	45
C-MOF-5	2119	1 M H_2SO_4	—	1	150	46
C-MOF-2	1378	1 M H_2SO_4	—	1	170	46
C-Zn-BTC	1326	1 M H_2SO_4	—	1	134	46
C-Zn-NDC	920	1 M H_2SO_4	—	1	114	46
C-Zn-ADA	513	1 M H_2SO_4	—	1	95	46
C-Zn-PAA	495	1 M H_2SO_4	—	1	110	46

4. Conclusions

In summary, we have used, for the first time, a microwave-assisted heating technique to efficiently prepare hierarchical porous carbon materials via the direct carbonization of ZIF-8 without any additional carbon sources. In this study, the surface areas and pore structures of the resulting carbons were easily controlled by the microwave carbonization temperature. The obtained ZIF-derived nanoporous carbons exhibit specific surface areas in the range of 384.4-947.5 m^2 g^{-1} and pore volumes in the range of 0.17-0.49 cm^3 g^{-1}. These porous carbon materials are mainly composed of micropores, but certain amounts of mesopores and macropores emerge due to the interconnection of nanoparticles when the carbonization temperature is higher than 800 ℃, which is quite different from carbon material prepared using traditional heating techniques. Of all the ZIF-derived nanoporous carbons examined, NPC-1000 possesses the highest percentage of mesopores and macropores and achieves the highest capacitance of 207.7 F g^{-1} at a current density of 0.1 A g^{-1}, due to its higher percentage of graphitic carbons and proper hierarchical pore structure. Moreover, NPC-1000 also shows excellent rate capability as a capacitor electrode material. The capacitance retention of NPC-1000 is 66.5% when the current density changes from 0.1A g^{-1} to 10A g^{-1}. Therefore, microwave-assisted heating is a very promising technique for the synthesis of MOF-derived nanoporous carbons. In particular, it can be used as a reference route for the preparation of hierarchical porous carbon materials. Future work will focus on improvements to provide improved microwave power control and allow the carbonization of other MOF precursors.

References

[1]   Winter M and Brodd R J 2004 What are batteries, fuel cells, and supercapacitors? *Chem Rev.* 104(10) 4245-70

[2]   Zhao Y, Liu J, Hu Y, Cheng H, Hu C, Jiang C and et al 2013 Highly compression-tolerant supercapacitor based on polypyrrole-mediated graphene foam electrodes *Adv Mater.* 25(4) 591-5

[3]   Wang D W, Liu S J, Jiao L, Fang G L, Geng G H and Ma J F 2017 Unconventional mesopore carbon nanomesh prepared through explosion-assisted activation approach: a robust electrode material for ultrafast organic electrolyte supercapacitors *Carbon.* 119 30-9

[4]   Wang D W, Liu S J, Fang G L, Geng G H and Ma J F 2016 From trash to treasure: direct transformation of onion husks into three-dimensional interconnected porous carbon frameworks for high-performance supercapacitors in organic electrolyte *Electrochim Acta.*, 216 405-11

[5]   Borchardt L, Oschatz M and Kaskel S 2014 Tailoring porosity in carbon materials for supercapacitor applications *Mater Horiz.* 1(2) 157-68

[6]   Wang D W, Liu S J, Jiao L and Fang G L 2017 A smart bottom-up strategy for the fabrication of porous carbon nanosheets containing rGO for high-rate supercapacitors in organic electrolyte *Electrochim Acta.* 252 109-18

[7]   Wang H and Gao Q 2009 Synthesis, characterization and energy-related applications of carbide-derived carbons obtained by the chlorination of boron carbide *Carbon.* 47(3) 820-8

[8]   Wang D W, Li F, Liu M, Lu G Q and Cheng H M 2008 3D aperiodic hierarchical porous graphitic carbon material for high-rate electrochemical capacitive energy storage *Angew Chem.* 47 373-6

[9]   Wang D W, Fang G L, Geng G H and Ma J F 2017 Unique porous carbon constructed by highly interconnected naonowalls for high-performance supercapacitor in organic electrolyte *Mater Lett.*, 189 50-3

[10]   Xia K, Gao Q, Jiang J and Hu J 2008 Hierarchical porous carbons with controlled micropores and mesopores for supercapacitor electrode materials *Carbon.* 46, 1718-26.

[11]   Largeot C, Portet C, Chmiola J, Taberna P L, Gogosti Y and Simon P 2008 Relation between the ion size and pore size for an electric double-layer capacitor *J Am Chem Soc.* 130 2730-1.

[12]   Wang D W, Wang Y T, Liu H W, Xu W and Xu L 2018 Unusual carbon nanomesh constructed by interconnected carbon nanocages for ionic liquid-based supercapacitor with superior rate capability *Chem Eng J.* 342 474-83

[13]   Thess A, Lee R, Nikolaev P, Dai H, Petit P, Robert J and et al 1996 Crystalline ropes of metallic carbon nanotubes *Science.* 273(5274) 483-7

[14]   Journet C, Maser W K, Bernier P, Loiseau A, Chapelle M L, Lefrant S and et al 1997 Large-scale production of single-walled carbon nanotubes by the electric-arc technique *Nature.* 388(6644) 756-8

[15]   Zheng B, Lu C, Gu G, Makarovski A, Finkelstein G and Liu J 2002 Efficient CVD growth of single-walled carbon nanotubes on surfaces using carbon monoxide precursor *Nano Lett.* 2(8) 895-8

[16]   Yang Q, Xu W, Tomita A and Kyotani T 2005 The template synthesis of double coaxial carbon nanotubes with nitrogen-doped and boron-doped multiwalls *J Am Chem Soc.* 127(25) 8956-7

[17]   Kim T W, Park I S and Ryoo R 2003 Intramolecular aromatic amination through iron-mediated nitrene transfer. Angew *Chem Int Ed.* 42(36) 4360-75

[18]   Ahmadpour A and Do D D 1996 The preparation of active carbons from coal by chemical and physical activation *Carbon.* 34(4) 471-9

[19] Fuertes A B 2003 Template synthesis of mesoporous carbons with a controlled particle size *J Mater Chem.* 13 3085-8

[20] Ma C, Shao X and Cao D 2012 Nitrogen-doped graphene nanosheets as anode materials for lithium ion batteries *J Mater Chem.* 22 8911-5

[21] Zhang P, Sun F, Xiang Z, Shen Z, Yun J and Cao D 2014 ZIF-derived in situ nitrogen-doped porous carbons as efficient metal-free electrocatalysts for oxygen reduction reaction *Energy Environ Sci.* 7(1) 442-50

[22] Liu B, Shioyama H, Akita T and Xu Q 2008 Metal-organic framework as a template for porous carbon synthesis *J Am Chem Soc.* 130(16) 5390-1

[23] Schoenecker P M, Carson C G, Jasuja H, Flemming C J and Walton K S 2012 Effect of water adsorption on retention of structure and surface area of metal-organic frameworks *Ind Eng Chem Res.* 51(18) 6513-9

[24] National Research Council National Materials Advisory Committee Microwave processing of materials National Research Council Washington DC National Academy Press 1994

[25] Menéndez J A, Arenillas A, Fidalgo B, Fernández Y, Zubizarreta L, Calvo E G and et al 2010 microwave-assisted heating processes involving carbon materials *Fuel Process. Technol.* 91 1-8

[26] Maruyama J, Sumino K, Kawaguchi M and Abe I 2004 Influence of activated carbon pore structure on oxygen reduction at catalyst layers supported on rotating disk electrodes *Carbon.* 42(15), 3115-21

[27] Sun L, Tian C, Fu Y, Yang Y, Yin J, Wang L and et al 2014 Nitrogen-Doped Porous Graphitic Carbon as an Excellent Electrode Material for Advanced Supercapacitors *Chem Eur J.* 20(2) 564-74

[28] Aleksandra S, Lavinia B, Véronique F, Lionel A, Ghouti M and Raphaël S 2014 Controlling ZIF-8 nano- and microcrystal formation and reactivity through zinc salt variations CrystEngComm. 16 4493-500

[29] Fletcher E A 1999 Solarthermal and solar quasi-electrolytic processing and separations: zinc from zinc oxide as an example *Ind Eng Chem Res.* 38(6) 2275-82

[30] Yang S J, Kim T, Im J H, Kim Y S, Lee K, Jung H and et al 2012 MOF-derived hierarchically porous carbon with exceptional porosity and hydrogen storage capacity *Chem Mater.* 24(3) 464-70

[31] Zhang J T, Yu L and Lou X W 2017 Embedding CoS2 nanoparticles in N-doped carbon nanotube hollow frameworks for enhanced lithium storage properties *Nano Res* 10(12) 4298-304

[32] Chen L F, Lu Y, Yu L and Lou X W 2017 Designed formation of hollow particle-based nitrogen-doped carbon nanofibers for high-performance supercapacitors *Energ Environ Sci.* 10 1777

[33] Rakhi R B, Chen W, Cha D and Alshareef H 2012 Nanostructured ternary electrodes for energy-storage applications *Adv Energy Mater.* 2(3) 381-9

[34] Chaikittisilp W, Hu M, Wang H J, Huang H S, Fujita T, Wu K C W and etal 2012 Nanoporous carbons through direct carbonization of a zeolitic imida zolate framework for supercapacitor electrodes *Chem. Commun.* 48 7259-61

[35] Bai F H, Xia Y D, Chen B L, Su H Q and Zhu Y Q 2014 Preparation and carbon dioxide uptake capacity of N-doped porous carbon materials derived from direct carbonization of zeolitic imidazolate framework *Carbon.* 75 213-26

[36] Wang Q, Yan J, Wang Y, Wei T, Zhang M, Jing X and et al 2014 Threedimensional flower-like and hierarchical porous carbon materials as high-rate performance electrodes for supercapacitors *Carbon.* 67 119-27

[37] Torad N L, Salunkhe R R, Li Y, Hamoudi H, Imura M, Sakka Y and et al 2014 Electric

double-layer capacitors based on highly graphitized nanoporous carbons derived from ZIF-67 *Chem Eur J.* 20 7895-900

[38] Sun L, Tian C, Fu Y, Yang Y, Yin J, Wang L and et al 2014 Nitrogendoped porous graphitic carbon as an excellent electrode material for advanced supercapacitors *Chem Eur J.* 20(2) 564-74

[39] Yang S J, Kim T, Lee K, Kim Y S, Yoon J and Park C R 2014 Solvent evaporation mediated preparation of hierarchically porous metal organic framework-derived carbon with controllable and accessible large-scale porosity *Carbon.* 71 294-302

[40] Wu H, Wang X, Jiang L, Wu C, Zhao Q, Liu X and et al 2013 The effects of electrolyte on the supercapacitive performance of activated calcium carbide-derived carbon *J Power Sources* 226 202-9

[41] Wu X, Hong X, Luo Z, Hui K S, Chen H, Wu J and et al 2013 The effects of surface modification on the supercapacitive behaviors of novel mesoporous carbon derived from rod-like hydroxyapatite template *Electrochim Acta.* 89 400-6.

[42] Ma C, Shao X and Cao D 2012 Nitrogen-doped graphene nanosheets as anode materials for lithium ion batteries. *J Mater Chem.* 22 8911-5.

[43] Li Y, Roy S, Ben T, Xu S and Qiu S 2014 Micropore engineering of carbonized porous aromatic framework (PAF-1) for supercapacitors application *Phys Chem Chem Phys.* 16(25) 12909-17